RIS Panel-assisted Enhanced Edge Computing for Batteryless IoT Sensors

Shakil Ahmed and Ahmed E. Kamal
Department of Electrical and Computer Engineering
Iowa State University, Ames, Iowa-50011, USA
Email: {shakil, kamal}@iastate.edu

***Abstract*—Reconfigurable intelligent surfaces (RISs) have emerged as efficient and cost-effective technique to enhance a great variety of possible performances of the Internet of Things (IoT) systems by reconfiguring the propagation environment. Motivated by this, we investigate the RIS-assisted edge computing systems for batteryless IoT sensors (b-IoT) under Rician fading channel conditions. We consider a fixed time frame divided into three slots. A b-IoT sensor harvests energy from radio frequency signals from a nearby base station (BS) during the first time slot. While performing local computation, the b-IoT sensor offloads computation bits to the BS and an IoT sensor using device-to-device communications protocol in the second and final time slots, respectively. An offloading ratio differentiates the fraction of computational bits, offloaded to BS and IoT sensors. We formulate the optimization problem with the convex sum of computational bits as objective function and energy consumption, offloading ratio, and energy harvesting constraints. We propose a gradient descent-based iterative algorithm to solve the optimization problem. Simulation assessments depict RIS panel-assisted edge computing and energy harvesting enhances the performance by more than 90% compared to the traditional baseline schemes, such as networks with no RIS panel.**

***Keywords*—RIS panel, passive elements, IoT sensor, edge computing, energy harvesting.**

I. Introduction

Through intelligent sensing and communication, Internet of Things (IoT) systems provide massive wireless connectivity for emerging technologies, such as smart cities, autonomous vehicles, etc. For example, mobile data traffic growth/year is about 30% between 2018 to 2024, with each sensor data usage from 6 to 23 GB/month [1]. These emerging technologies require continuous information updates and complex computational processing. This issue becomes even more critical for batteryless IoT (b-IoT) sensors due to their communications and on-board computational requirements under energy resources constraints. Edge computing, providing computing execution resources for sensors close to end-users, and energy harvesting are viable solutions to overcome the computational complexity with limited on-board energy constraints of b-IoT sensors.

b-IoT sensors encounter considerable challenges of realizing energy-efficient, low-performance, and low latency processors [2]. External power sources must provide energy to b-IoT sensors in order to support their operations. Given the complexity and higher expense, harvesting energy from external sources like solar or wind is not always viable solution approach. Energy harvesting, therefore, from nearby base station (BS) radio frequency (RF) signals attracts growing interest, thanks to converting harvested RF signals into electricity. Hence, energy harvesting provides a stable and controllable energy source to prolong b-IoT sensors' lifetime.

Reconfigurable intelligent surfaces (RISs) may have passive elements to control the reflection angle and attenuation of the incident signals. The receiving nodes receive stronger signals and enhance the performance. Therefore, adding an RIS panel makes energy harvesting and channel modeling robust by creating intelligent radio environments. Hence, enabling propagation paths to be co-designed with physical layer signaling [3]. Incorporating RIS panels into the networks further maximizes the channel gain between nodes due to artificial incident signals reconfiguration.

The RIS panels can be used to enhance b-IoT systems performance. However, the benefits of RIS panels to edge computing systems for b-IoT sensors receive little attention in the literature. For example, the RIS panel assisted-edge computing was studied to leverage edge computing during the offloading time [4]. The authors in [5] investigated the energy consumption model to compute bits and associated delay for assessing RIS-assisted edge computing systems. The sum computation bits are investigated to measure system performance to assess the edge computing system. The authors in [6] investigated the RIS-assisted edge computing maximization to achieve an optimal resource allocation. However, they do not consider the on-board energy constraint of the nodes. In [7], the authors proposed a RIS panel-assisted edge computing to design an efficient computing algorithm from resource-constrained mobile devices. The authors in [8] proposed power transfer relaying protocols for energy-constrained relay nodes by using power splitting and time switching receivers. However, the authors did not deploy the RIS panel and efficient edge computing in their model.

The contribution of this paper is as follows: We propose a multi-purpose use of the RIS panel with passive elements powered by harvested energy, as shown in Fig. 1. We model all possible communications links using Rician fading without/through the RIS panel between communicating nodes.

To assess the RIS panel-assisted edge computing system, we optimize the sum computation bits to leverage the benefits of the RIS panel over the computation performed. We divide a fixed duration time frame divided into three optimal time slots, named as phases, which are summarized as follows: *(1) Phase I:* b-IoT sensor, S harvests energy from nearby BS RF signals during the first time slot. For local and offloaded computation, an energy efficiency factor determines the fraction of energy harvested by S. *(2) Phase II:* S offloads computation bits to the BS in the second optimal time slot. *(3) Phase III:* S then offloads the remaining computation bits to IoT sensor, D using a D2D communications protocol in the last time slot. We propose a gradient descent based-iterative algorithm by taking the Lagrangian multiplier into account to solve the non-convex optimization problem.

In the paper organization, we describe the system model, the optimization problem, its solution, the simulation results, and the conclusion in Section I - IV, respectively.

II. System Model

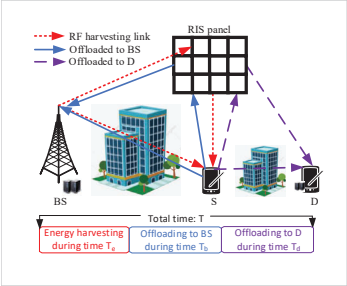

Fig. 1: System model

We consider IoT systems with batteryless sensors, assisted by an RIS panel, where each device is equipped with a single antenna element and edge computing capabilities. Each of these IoT sensors is referred to b-IoT. The RIS panel, having N passive elements, is powered by energy harvested from BS RF signals and y is each contributing element power consumption. We assume that the passive elements of the RIS panel are ideal and control the incident signals' reflection angle and phase shift. b-IoT sensor, S, has a computation task, which may be processed locally or offloaded to nodes, such as a BS and an IoT sensor, D, followed by an offloading ratio. The total time is divided into repeating time frames, and each frame with duration, T, is divided into three optimal slots, namely T_e, T_b, and T_d. S harvests energy from BS RF signals during T_e time. Using the harvested energy, S offloads computation tasks to the BS during the T_b time slot and D during the T_d time slot. Table I summarizes the parameters used in the paper.

TABLE I: List of symbols used in the paper

Symbol	Description	Symbol	Description
$w_{\{.\}}$	Variables	$c_{\{.\}}, \omega$	Constants
T	Total time	$\lambda_{\{.\}}$,	Variables
p_b	BS power	$m_{\{.\}}$	Variables
λ^r	Wavelength	h_{bs}, h_{sb}	BS-S gains
N	RIS elements	$B_{\{.\}}$	Computation bits
K	Rician factor	$W_{\{.\}}$	Bandwidth
$\mathbf{e}$	Harvested energy	α, β, γ	Reflection coefficient
ζ	Efficiency factor	$\delta_{[.]}$	Path loss exponent
y	Each element power	$\Theta^{\{.\}}$	Diagonal matrix
f	Fractional number	$v_{\{.\}}$	Comm. overhead
ρ	Offloading ratio	$p_{c,bs}$	S power circuit to BS
e_m	Min. harv. energy	$T_{\{.\}}$	Time for Phase I-III
$\mathbf{h_{SR,RS}}$	S-RIS gains	$\theta^{\{.\}}$	RIS phase shift
$\mathbf{h_{RD}}$	RIS-D gains	p, q, r	RIS in Phase I-III
C_c	CPU cycle/bit	$p_{c,d2d}$	S power circuit to D
$\mathbf{h_B}$	Gains between S-BS	P, Q, R	Variables
Φ	Dual function	$\mathcal{L}$	Lagrangian multiplier
$\mathbf{h_D}$	Gains bet^n S-D	$\mathbf{h_{EH}}$	Gains at energy harves.
h_{sd}	S-D gain	d	Midpoint array distance
$\mathbf{h_{BR,RB}}$	BS-RIS gain	$[.]^\dagger$	Conjugate matrix
C_e	Eff. capacitance co-eff.	C_f	Centre frequency

A. Phase I: Energy harvesting from BS RF signals

1) RIS panel: Passive elements of the RIS panel are designed to reflect the incident signals to the destination of interest. Each passive element is smaller than the wavelength, λ^r. The authors in [9] showed that a passive element is a square patch of size $\frac{\lambda^r}{5} \times \frac{\lambda^r}{5}$, where λ^r is the signal wavelength, to behave as diffusers with no strong intrinsic guidance. The elements adjust the reflection coefficient to reflect the signals with nearly the same gain into the directions of interest. We express the RIS panel properties in a diagonal $N \times N$ matrix during the energy harvesting period as follows: $\mathbf{\Theta^e} = \text{diag}(\alpha_1 e^{j\theta_1^e}, \alpha_2 e^{j\theta_2^e}, ..., \alpha_N e^{j\theta_N^e})$, where $\alpha_i \in [0, 1]$ is amplitude reflection coefficient and θ_i^e is the RIS passive elements phase-shift.

2) Channel gain: We consider the channel gain from the BS to S, the BS to RIS, and RIS to S are h_{bs}, $\mathbf{h_{BR}} \in \mathbb{C}^{N\times 1}$, and $\mathbf{h_{RS}} \in \mathbb{C}^{N\times 1}$, respectively. The effective channel gain from S to the BS is:

$$\mathbf{h_{EH}} = h_{bs} + \mathbf{h_{BR}^\dagger \Theta^e h_{RS}} \tag{1}$$

The direct link from the BS to S channel gain, by adopting Rician fading, is given as follows:

$$h_{bs} = \frac{\sqrt{\beta_{bs}^{-1}}}{\sqrt{K+1}}(\sqrt{K} h_{bs}^{los} + h_{bs}^{nlos}) \tag{2}$$

where $\beta_{bs} = \frac{16\pi^2 d^{\delta_1}}{\lambda^2}$. δ_1 is the path loss exponent and d is communicating node midpoint array distance. The elements of h_{bs}^{nlos}, and h_{bs}^{los} are independently and identically distributed (i.i.d.) according to $\mathcal{CN}(0, 1)$. $K \in [0, +\infty)$ is Rician factor. The channel gains for given $\mathbf{\Theta^e}$ is:

$$\mathbf{h_{BR}^\dagger \Theta^e h_{RS}} = \sum_{n=1}^{N} \alpha_n e^{j\theta_n^e} [\mathbf{h_{BR}^\dagger}]_n [\mathbf{h_{RS}}]_n \tag{3}$$

Phase shift, θ_n^e is selected in the sum to be the same phase of h_{bs}. θ_n^e, therefore, is expressed as [10]:

$$\theta_n^e = \arg(h_{bs}) - \arg([\mathbf{h_{BR}^\dagger}]_n [\mathbf{h_{RS}}]_n) \tag{4}$$

3) Energy harvesting: We assume that b-IoT sensor has compatible hardware components required for energy harvesting. S leverages energy harvesting from BS RF signals to support its operations while also decoding BS RF signals from data recipients. The received BS RF signals is converted into direct current through a rectifier. The rectifier consists of the passive low-pass filter and Schottky diode. Harvested energy from BS RF signals during T_e is:

$$\begin{aligned}\mathbf{e} &= \max_{\theta_1^e,\ldots,\theta_N^e} \zeta T_e p_b (h_{bs} + \mathbf{h}_{\mathbf{BR}}^{\dagger} \mathbf{\Theta^e} \mathbf{h}_{\mathbf{RS}})^2 \\ &= \zeta T_e p_b (h_{bs} + p[\mathbf{h}_{\mathbf{BR}}^{\dagger}]_n [\mathbf{h}_{\mathbf{RS}}]_n)^2 \end{aligned} \tag{5}$$

where p_b is BS transmit power. T_e is the time used during energy harvesting. ζ is energy efficiency factor. $[.]^{\dagger}$ is conjugate transpose matrix. p is contributing elements from N.

4) Local Computation: The number of locally computed bits is [11]:

$$B_l = (T_b + T_d)\frac{C_f}{C_c} \tag{6}$$

where T_b and T_d are the computation offloading time for BS and D, respectively. C_c is the CPU cycle number per bit required for local computation. C_f is the center frequency.

5) Energy consumption for local computation: We assume no overhead associated with the partition of computation bits. The energy consumed for local computation is [11]:

$$E_l = (T_b + T_d) C_e C_f^3 \tag{7}$$

where C_e defines chip architecture-depended effective capacitance coefficient of the processor.

B. Phase II: computation offloading to BS

1) RIS properties: We express the RIS properties during the offloading to BS as $N \times N$ diagonal matrix as follows: $\mathbf{\Theta^b} = \text{diag}(\beta_1 e^{j\theta_1^b}, \beta_2 e^{j\theta_2^b}, .., \beta_k e^{j\theta_N^b}, \beta_N e^{j\theta_N^b})$, where $\beta_i \in [0,1]$ is the amplitude reflection coefficient and θ_i^b is passive elements phase-shift. q is contributing elements from N.

2) Channel gain: We consider channel gain from S to the BS, S to RIS, and RIS to BS are h_{sb}, $\mathbf{h_{SR}} \in \mathbb{C}^{N\times 1}$, and $\mathbf{h_{RB}} \in \mathbb{C}^{N\times 1}$, respectively. Channel gain from BS-to-S is:

$$\mathbf{h_B} = h_{sb} + \mathbf{h_{SR}^{\dagger}} \mathbf{\Theta^b} \mathbf{h_{RB}} \tag{8}$$

We adopt the Rician fading but in the opposite Phase from II-A2, which is defined as h_{sb}. For any given $\mathbf{\Theta^b}$, we have gains as $\mathbf{h}_{\text{SR}}^{\dagger} \mathbf{\Theta^b} \mathbf{h}_{\text{RB}} = \sum_{n=1}^{N} \alpha_n e^{j\theta_n^e} [\mathbf{h}_{\text{SR}}^{\dagger}]_n [\mathbf{h}_{\text{RB}}]_n$. Phase shift, θ_n^b is selected in the sum to be the same Phase of h_{bs}. θ_n^b is expressed as $\theta_n^b = \arg(h_{sb}) - \arg([\mathbf{h}_{\text{SR}}^{\dagger}]_n [\mathbf{h}_{\text{RB}}]_n)$.

3) Energy consumption for BS: After computation, the BS sends back the outcome to S. The BS has sufficient CPU capability to assume that offloading time is negligible since the BS may have high power and computation capability. Authors in [11] suggest that Computation and downloading steps have a negligible effect on the computation process. We, therefore, adopt these assumptions in our model. The consumed energy to offload to the BS is expressed as follows:

$$E_b = T_b(\frac{f\mathbf{e}}{T_b} + p_{c,bs}) \tag{9}$$

where $p_{c,bs}$ defines circuit power of S during offloading to the BS. f defines the fraction of the harvested energy used to compute offloaded bits to BS. $\mathbf{e}$ is defined from (5).

4) Computation at BS: The offloading Phase has offloading, computing, and downloading steps. The computation offloading tasks of S include raw data encryption and packet header. S offloads the maximum bits to the BS during T_b, which is expressed as follows:

$$\begin{aligned} B_b &= \max_{\theta_1^b,\ldots,\theta_N^b} \rho \frac{T_b W_1}{v_b} \log_2\left(1 + \frac{f\mathbf{e}}{T_b} \frac{\mathbf{h_B}^2}{\sigma^2}\right) \\ &= \rho \frac{T_b W_1}{v_b} \log_2\left(1 + \frac{f\mathbf{e}}{T_b} \frac{\mathbf{h_B^{'}}^2}{\sigma^2}\right) \end{aligned} \tag{10}$$

where $\mathbf{h_B^{'}} = h_{sb} + q[\mathbf{h_{SR}^{\dagger}}]_n [\mathbf{h_{RB}}]_n$. $v_b > 1$ is the communication overhead. W_1 is the bandwidth. ρ is the computation offloading ratio. σ^2 denotes the noise power.

C. Phase III: computation offloading to D

1) RIS properties: We express the RIS properties for passive elements to S during the offloading to the D as $N \times N$ diagonal matrix as follows: $\mathbf{\Theta^d} = \text{diag}(\gamma_1 e^{j\theta_1^d}, \gamma_2 e^{j\theta_2^d}, .., \gamma_N e^{j\theta_N^d})$, where $\gamma_i \in [0,1]$ is the fixed amplitude reflection coefficient and θ_i^d is the phase-shift. r is the number of contributing elements from N.

2) Channel gain: Let the channel matrix from S to D, S to RIS, and RIS to D are h_{sd}, $\mathbf{h_{SR}} \in \mathbb{C}^{N\times 1}$, and $\mathbf{h_{RD}} \in \mathbb{C}^{N\times 1}$, respectively. Thus, the channel gain from the BS to S is expressed as follows:

$$\mathbf{h_D} = h_{sd} + \mathbf{h_{SR}^{\dagger}} \mathbf{\Theta^d} \mathbf{h_{RD}} \tag{11}$$

The direct link from the BS to S channel gain, by adopting Rician fading, is given as follows:

$$h_{sd} = \frac{\sqrt{\beta_{sd}^{-1}}}{\sqrt{K+1}} (\sqrt{K} h_{sd}^{los} + h_{sd}^{nlos}) \tag{12}$$

where $\beta_{sd} = \frac{16\pi^2 d^{\delta_2}}{\lambda^2}$. δ_2 is the path loss exponent. The elements of h_{sd}^{nlos}, and h_{sd}^{los} are i.i.d. according to $\mathcal{CN}(0,1)$. $K \in [0, +\infty)$ is Rician factor. For any given $\mathbf{\Theta^d}$, we have gains as $\mathbf{h}_{\text{SR}}^{\dagger} \mathbf{\Theta^d} \mathbf{h}_{\text{RD}} = \sum_{n=1}^{N} \alpha_n e^{j\theta_n^e} [\mathbf{h}_{\text{SR}}^{\dagger}]_n [\mathbf{h}_{\text{RD}}]_n$. Phase shift, θ_n^e is selected in the sum to be the same Phase of h_{bs}. θ_n^d is expressed as $\theta_n^d = \arg(h_{sd}) - \arg([\mathbf{h}_{\text{SR}}^{\dagger}]_n [\mathbf{h}_{\text{RD}}]_n)$.

3) Energy consumption for D: S offloads computation bits to D, followed by D2D communications protocol, during T_d. The consumed energy to offload to D is:

$$E_d = T_d(\frac{(1-f)\mathbf{e}}{T_d} + p_{c,d2d}) \tag{13}$$

where $p_{c,d2d}$ is circuit power of S during offloading to D.

4) Computation at D: S offloads the remaining bits to D, which is expressed as follows:

$$\begin{aligned} B_d =& \max_{\theta_1^d,..,\theta_N^d} (1-\rho)\frac{T_b W_2}{v_d}\log_2\left(1+\frac{(1-f)\mathbf{e}}{T_d}\frac{\mathbf{h_D}^2}{\sigma^2}\right) \\ =& (1-\rho)\frac{T_b W_2}{v_d}\log_2\left(1+\frac{(1-f)\mathbf{e}}{T_d}\frac{\mathbf{h_D}^{'2}}{\sigma^2}\right) \end{aligned} \tag{14}$$

where $\mathbf{h_D}^{'} = h_{sd} + r[\mathbf{h_{SR}}^{\dagger}]_n[\mathbf{h_{RD}}]_n$. $v_d > 1$ indicates the communication overhead. W_2 is the bandwidth.

III. Optimization Problem

We jointly optimize time allocations, T_e, T_b, T_d, number of RIS elements, and the offloading ratios with the objective of maximizing the sum of computation bits is:

$$\max_{p,q,r,T_e,T_b,T_d,\rho} B_l + B_b + B_d \tag{15a}$$

$$\text{s.t. } e_t \le \zeta T_e p_b (h_{bs} + p[\mathbf{h_{BR}}^{\dagger}]_n[\mathbf{h_{RS}}]_n)^2 \tag{15b}$$

$$py \le (N-p)\mathbf{e},\ qy \le (N-q)\mathbf{e},\ ry \le (N-r)\mathbf{e} \tag{15c}$$

$$0 \le \rho \le 1 \tag{15d}$$

$$p \le N, q \le N, r \le N \tag{15e}$$

$$(7),\ (9),\ (13)$$

The objective function in (15a) maximizes both locally and offloaded computed bits. The energy harvesting model is shown in (15b), where e_t is the threshold. Power consumed by RIS passive elements, p, q, and r during Phase I, II, and III, respectively, are described in (15c). The offloading ratio is bounded in (15d).

IV. Proposed Solution

Problem (15) is not convex due to (15a) - (15c) containing the coupling of optimizing variables, making (15) challenging to solve. We tackle the coupling of non-convex energy harvesting from BS RF signal constraint in (15b) by defining as follows: $e_t \le T_e \mathbf{e_n}$, where $\mathbf{e_n} = \zeta p_b (h_{bs} + p[\mathbf{h_{BR}}^{\dagger}]_n[\mathbf{h_{RS}}]_n)^2$. We transform (15) as follows:

$$\max_{p,q,r,T_e,T_b,T_d,\rho,\mathbf{e_n},w_1,w_2} B_l + w_b + w_d \tag{16a}$$

$$\text{s.t. } w_b \le B_b,\quad w_d \le B_d \tag{16b}$$

$$py \le (N-p)T_e\mathbf{e_n} \tag{16c}$$

$$qy \le (N-q)T_e\mathbf{e_n} \tag{16d}$$

$$ry \le (N-r)T_e\mathbf{e_n} \tag{16e}$$

$$e_t \le T_e\mathbf{e_n} \tag{16f}$$

$$(7),\ (9),\ (13),\ (15d),\ (15e)$$

where w_b and w_d are newly introduced variables.

Lemma 1: Let $\{\lambda_b^*\}$, $\{\lambda_d^*\}$, $\{p^*\}$, $\{q^*\}$, $\{r^*\}$, $\{T_e^*\}$, $\{T_b^*\}$, $\{T_d^*\}$, $\{\rho^*\}$, $\{w_b^*\}$, $\{w_d^*\}$ be the optimal variables of (16), where λ_b, λ_d, w_b and w_d are auxiliary variables. There must be $\{\lambda_b^*\}$, $\{\lambda_d^*\}$ so that optimizing variables satisfy Karush-Kuhn-Tucker condition such that $\lambda_b^* = \lambda_b, \lambda_d^* = \lambda_d, w_b = w_b^*, w_d = w_d^*$. We analyze $w_b \le B_b$ from (16b) as follows:

$$0 \le \frac{B_b^n}{T_b} \tag{17}$$

where $B_b^n = 1 + c_2 T_e \mathbf{h_B}^{'2} - T_b(1 - 2^{\frac{w_b}{m_1 c_1}})$. $c_1 = \frac{W_1}{v_b}$, $c_2 = \frac{f\mathbf{e_n}}{\sigma^2}$. We define $m_1 = \rho T_b$ to address the coupling variables issue. We reformulate $w_d \le B_d$ from (16b) as follows:

$$0 \le \frac{B_d^n}{T_d} \tag{18}$$

where $B_d^n = 1 + c_4 T_e \mathbf{h_D}^{'2} - T_d(1 - 2^{\frac{w_d}{m_2 c_3}})$, $c_3 = \frac{W_2}{v_b}$, $c_4 = \frac{(1-f)\mathbf{e_n}}{\sigma^2}$. We define $m_2 = (1-\rho)T_d$ to address the coupling variables issue. Similarly, we reformulate (16c) - (16e) as follows:

$$\begin{aligned} &0 \le \frac{(NT_e - P)\mathbf{e_n} - py}{py},\ 0 \le \frac{(NT_e - Q)\mathbf{e_n} - qy}{qy}, \\ &0 \le \frac{(NT_e - R)\mathbf{e_n} - ry}{ry} \end{aligned} \tag{19}$$

where $P = T_e p$, $Q = T_e q$, $R = T_e r$ are defined to address the coupling variables issues and also for rotational brevity. We reformulate (16) using (17) - (19) as follows:

$$\max_{\substack{p,q,r,P,Q,R,T_e,\\ T_d,T_b,m_1,m_2,\mathbf{e_n}}} \lambda_l B_l + \lambda_b(B_b^n - w_b T_b) + \lambda_d(B_d^n - w_d T_d) \tag{20a}$$

$$\text{s.t. } 0 \le \lambda_p((NT_e - P)\mathbf{e_n} - py) - w_p py) \tag{20b}$$

$$0 \le \lambda_q((NT_e - Q)\mathbf{e_n} - qy) - w_q qy) \tag{20c}$$

$$0 \le \lambda_r((NT_e - R)\mathbf{e_n} - ry) - w_r ry) \tag{20d}$$

$$(7),\ (9),\ (13),\ (15e),\ (16f)$$

$(\{p^*\},\{q^*\},\{r^*\},\{P^*\},\{Q^*\},\{R^*\},\ \{T_e^*\},\ \{T_d^*\},\{T_b^*\},\ \{m_1^*\},\ \{m_2^*\})$ satisfy for $\lambda_i = \lambda_i^*$, $w_i = w_i^*$, where $i \in \{l, b, d, p, q, r, P, Q, R\}$. λ_i and w_i should satisfy the following conditions.

$$\begin{aligned} &\lambda_b = \frac{1}{T_b}, \lambda_d = \frac{1}{T_d}, \lambda_p = \frac{1}{py}, \lambda_q = \frac{1}{qy}, \lambda_r = \frac{1}{ry}, w_b = \frac{B_b^n}{T_b}, w_d = \\ &\frac{B_d^n}{T_d}, w_p = \frac{(NT_e - P)\mathbf{e_n} - py}{py}, w_p = \frac{(NT_e - P)\mathbf{e_n} - py}{py}, \\ &w_q = \frac{(NT_e - Q)\mathbf{e_n} - qy}{qy}, w_r = \frac{(NT_e - R)\mathbf{e_n} - ry}{ry} \end{aligned} \tag{21}$$

Proof: We prove *Lemma 1* by considering Lagrange function of (20). A detailed proof is shown in [12].

We apply *Lemma 1* to achive the solutions of λ_i, and w_i from (20). Hence, Lagrange function of (20) is:

$$\begin{aligned} \mathcal{L} =& \lambda_l B_l + \lambda_b(B_b^n - w_b T_b) + \lambda_d(B_d^n - w_d T_d) - \lambda_P((NT_e \\ &- P)\mathbf{e_n}) - \lambda_p(py - w_p py) - \lambda_Q((NT_e - Q)\mathbf{e_n}) - \lambda_q(\\ &qy - w_q qy) - \lambda_R((NT_e - R)\mathbf{e_n}) - \lambda_r(ry - w_r ry) - \\ &\lambda_{eh}(e_t - T_e\mathbf{e_n}) - \lambda_{ec}(E_l + E_b + E_d) \end{aligned} \tag{22}$$

We define λ_{ec} and λ_{eh} as non-negative Lagrange multipliers for (16f). We conclude that it is easy to prove that (20) is

convex for a given λ_i and w_i. A strong duality exists between primary and dual problems. Hence, (20) is equivalent to the solution of the dual problem. This transformation is expressed as follows:

$$\min_{\lambda_i, w_i} \Phi(\lambda_i, w_i) \tag{23}$$

where $i \in \{l, b, d, p, q, r, P, Q, R\}$ and

$$\Phi(\lambda_i, w_i) = \max_{\substack{p,q,r,P,Q,R,T_e,\\ T_b,T_d,m_1,m_2}} \mathcal{L} \tag{24}$$

In the next step, we find the solution of λ_i, w_i, and $\mathcal{L}$. The gradient descent method guides $\mathcal{L}$ and the auxiliary variables to be updated. Using (22), we maximize the dual function as follows:

$$\begin{aligned}\Phi = \max_{\substack{p,q,r,P,Q,R,T_e,\\ T_b,T_d,m_1,m_2}} & \lambda_l B_l + \lambda_b B_b^n + \lambda_d B_d^n - \lambda_{ec} E_l - \lambda_{ec} E_b \\ & - \lambda_{ec} E_d \lambda_b - w_b T_b - \lambda_d w_d T_d - \mathbf{e_n} \lambda_P (NT_e - P) - \lambda_Q \mathbf{e_n} \\ & (NT_e - Q) - \lambda_R \mathbf{e_n} (NT_e - R) - \lambda_p py - \lambda_q qy - \lambda_r ry + \omega\end{aligned} \tag{25}$$

where ω is the sum of values irrelevant to the optimizing variables. We achieve the optimal solution by taking the first order derivative of Lagrange function as follows:

$$\begin{aligned} & p^* = \lambda_p y, \ q^* = \lambda_q y, \ r^* = \lambda_r y, P^* = \lambda_P \mathbf{e_n}, \\ & Q^* = \lambda_Q \mathbf{e_n}, \ R^* = \lambda_R \mathbf{e_n} \end{aligned} \tag{26}$$

$$\begin{aligned} T_d^* = \lambda_l \frac{C_f}{C_e} + \lambda_d (1 - 2^{\frac{B_d^t}{m_2^* c_3}}) + \lambda_{ec} (C_e C_f^3 - (1 - f) \\ \mathbf{e_n} - \lambda_1) - \lambda_d w_d \end{aligned} \tag{27}$$

$$\begin{aligned} T_b^* = \lambda_l \frac{C_f}{C_e} + \lambda_b (1 - 2^{\frac{B_b^t}{m_1^* c_1}}) + \lambda_{ec} (C_e C_f^3 - f \\ \mathbf{e_n} - \lambda_2) - \lambda_b w_b \end{aligned} \tag{28}$$

$$\begin{aligned} T_e^* = & \lambda_b c_2 \mathbf{h_B}^{'\,2} + \lambda_d c_4 \mathbf{h_D}^{'\,2} \lambda_{ec} (f \mathbf{e_n} - \lambda_3 T_b^* - (1 - f) \\ & (\mathbf{e_n} - \lambda_4 T_d^*) + \lambda_{eh} \mathbf{e_n} - \lambda_P N \mathbf{e_n} \\ & - \lambda_Q N \mathbf{e_n} - \lambda_R N \mathbf{e_n} \end{aligned} \tag{29}$$

Plugging the value of (26) - (29) in (20) results a linear maximization problem. The optimization problem, therefore, can be solved using interior-point methods [13]. We summarize the solution in an algorithm as follows:

Algorithm 1 Enhanced Edge Computing Algorithm

1: **Initialize**: $i = 0$, λ_i, and w_i
2: **repeat**
3: Achieve p^*, q^*, r^* from (26), T_d^* from (27), T_b^* from (28), and T_e^* from (29)
4: Solve (20) using $p^*, q^*, r^*, T_d^*, T_b^*, T_e^*$.
5: Update Lagrange multipliers and auxiliary variables from $i \rightarrow i + 1$
6: Output of the optimal enhanced edge computing
7: **until** convergence

Updating the Lagrange variables has the complexity of $\mathcal{O}(K^2)$ due to the $3K + 1$ number of variables. $\mathcal{O}(z)$ means that the upper limit of complexity increases with an order of z. Hence, the complexity of Algorithm 1 is $\mathcal{O}(K^7)$. Algorithm 1 guarantees the convergence [14].

V. Simulation Results

We show simulation results in this section. The BS, S, D, and RIS panels are deployed at fixed locations. The distance between two communicating nodes determines their corresponding channel gains. We consider $T \in \{50, 100, 150, 200, 250\}$ ms, $N \in \{50, 100, 150, 200, 250\}$, $\sigma^2 = -94$ dBm, $\zeta = [0, 1)$, $p_b = 2$ W, $e_m = 0.1$ mJ, and $v_b = v_d = 2$.

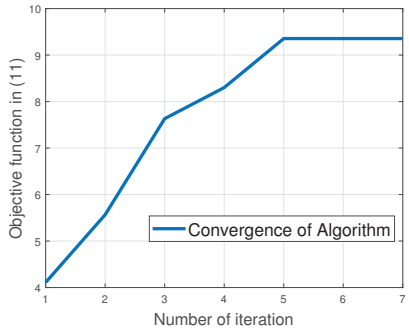

Fig. 2: Convergence performance

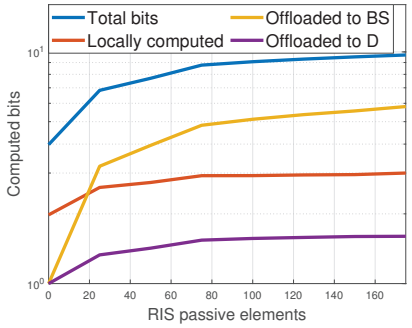

Fig. 3: Bits computation

Fig. 2 shows that the convergence of the optimization problem is fast and occurs at the fifth iteration. Fig. 3 shows the number of computed bits when we vary the number of passive elements of the RIS panel and compare it to the case when the system does not deploy an RIS panel, i.e., $N = 0$. The RIS panel plays a critical role in offloading an optimal number of bits to the BS and D since we adopt a Rician fading channel between S and the BS and D. With no RIS panel, S offloads a trivial fraction of computational bits to other nodes due to adverse channel conditions. Hence S primarily performs local computation and computes only a tiny fraction of bits. When the number of passive elements increases, S offloads bits to other nodes. Due to BS's higher computation handling capacity than D, the BS computes a higher fraction of offloaded bits. We find that around 90% of

computational bits are performed by S and the BS, while D performs small fraction computations.

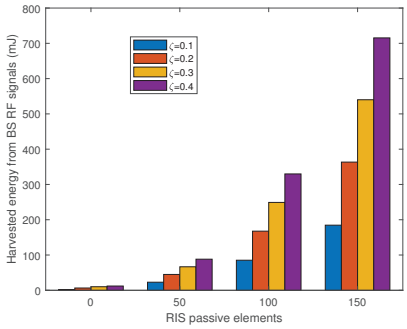

Fig. 4: Energy harvesting from BS RF signals

In Fig 4, we show the performance of harvested energy, in the form of a histogram, for the various number of passive elements and compare it to the case when N=0. A fewer RIS panel passive elements reduces the number of micro-controllers used for RIS. Eventually, it becomes less expensive with less hardware complexity. However, a higher number of passive elements guarantees a higher fraction of energy from BS RF signals. Fig. 4 also shows that a higher amount of energy is harvested from BS RF signals for the optimal number of passive elements and efficiency factors. For example, $N = 150$ defines our proposed algorithm to find the optimal number of passive elements between $N = 0$ to 150 to harvest the optimal fraction of BS RF signals. Even for higher ζ, energy harvesting does not increase when $N = 0$. This is because we adopt Rician fading between BS-to-S, hence, weakening the received signals significantly.

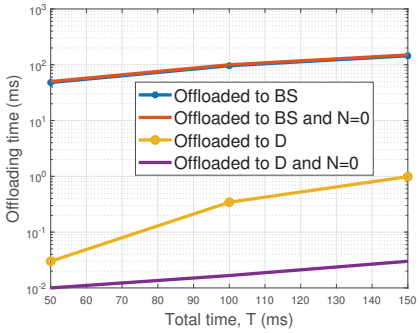

Fig. 5: Computational offloading time vs. total time

In Fig. 5, computational offloading time varies for total time and compare it $N = 0$. Due to the more significant number of passive elements, all possible links are reflected by the RIS panel to the IoT sensors. The offloading time increases the total time frame increases. This is obvious because higher total time allows S to offload more bits than local computation. On the other hand, the remaining time is utilized for energy harvesting from BS RF signals.

VI. Conclusion

We study the RIS panel-assisted edge computing systems for b-IoT sensors in an adverse Rician fading channel condition. We investigate the effect of RIS passive elements on energy harvesting and the offloading computation performance for a b-IoT sensor for a given time frame, divided into three optimal slots. RIS panel passive elements adjust the phase shift and reflect the incident signals to the receiving nodes, significantly enhancing energy harvesting and edge computation performance. The b-IoT sensor harvests energy from RF signals from a nearby BS for use in computation and communications. Then b-IoT performs the local computation and offloads the remaining bits to the BS in the second time slots and another IoT sensor in the last time slot, following an offloading ratio. An optimization problem is formulated to maximize the sum of computational bits, subject to energy consumption at each stage, offloading ratio, and passive elements of RIS. We propose an iterative algorithm to achieve optimal solutions to the non-convex optimization problem. Simulation results show the advantage of edge computing RIS panel assisted systems for b-IoT sensors.

References

[1] Ericsson. *Ericsson Mobility Report.* Accessed: Jun., 2019. [Online].

[2] Y. Mao, C. You, J. Zhang, K. Huang, and K. B. Letaief, "A survey on mobile edge computing: The communication perspective," *IEEE Commun. Surveys Tuts.*, vol. 19, no. 4, pp. 2322–2358, 2017.

[3] M. D. Renzo et al., "Smart radio environments empowered by reconfigurable AI meta-surfaces: An idea whose time has come," *EURASIP J. Wireless Commun. Netw.*, vol. 2019, p. 129, May 2019.

[4] T. Bai, C. Pan, Y. Deng, M. Elkashlan, A. Nallanathan, and L. Hanzo, "Latency minimization for intelligent reflecting surface aided mobile edge computing," *IEEE J. Sel. Areas Commun.*, vol. 38, no. 11, pp. 2666–2682, Jul. 2020.

[5] T. Bai, C. Pan, H. Ren, Y. Deng, M. Elkashlan, and A. Nallanathan, "Resource allocation for intelligent reflecting surface aided wireless powered mobile edge computing in OFDM systems," 2020. [Online]. Available: https://arxiv.org/abs/2003.05511.

[6] S. Hua and Y. Shi, "Reconfigurable intelligent surface for green edge inference in machine learning," in *Proc. IEEE Globecom Workshops (GC Wkshps)*, 2019, pp. 1–6.

[7] S. Hua, Y. Zhou, K. Yang, Y. Shi, and K. Wang, "Reconfigurable Intelligent Surface for Green Edge Inference," *IEEE Trans. Green Commu. and Netwo.*, vol. 5, no. 2, pp. 964-979, June 2021

[8] A. Nasir X. Zhou, S. Durrani, and R. Kennedy, "Relaying protocols for wireless energy harvesting and information processing," *IEEE Trans. Wireless Commun.*, vol. 12, no. 7, pp. 3622–3636, Jul. 2013.

[9] Ö. Özdogan, E. Björnson, and E. G. Larsson, "Intelligent reflecting surfaces: Physics, propagation, and path loss modeling," *IEEE Wirele. Commun. Lett.*, vol. 9, no. 5, pp. 581–585, 2020.

[10] E. Bjornson, O. Ozdogan, and E. G. Larsson, "Intelligent Reflecting Surface Versus Decode-and-Forward: How Large Surfaces are Needed to Beat Relaying?," *IEEE Wirel. Commun. Lett.*, vol. 9, no. 2, pp. 244-248, Feb. 2020.

[11] F. Zhou and R. Q. Hu, "Computation efficiency maximization in wireless-powered mobile edge computing networks," *IEEE Trans. Wireless Commun.*, vol. 19, no. 5, pp. 3170–3184, May 2020.

[12] Y. Jong, "An efficient global optimization algorithm for nonlinear sum-of-ratios problem," May 2012. [Online]. Available: http://www.optimizationonline. org/DBFILE/2012/08/3586.pdf

[13] A. Bakry, R. Tapia, T. Tsuchiya, and Y. Zhang, "On the formulation and theory of the Newton interior-point method for nonlinear programming", *Journ. Optim. Theor. Appl.* vol. 89, pp. 507–541, 1996

[14] K. Yuan, Q. Ling, and W. Yin, "On the convergence of decentralized gradient descent", *SIAM Journ. Optim.,*, vol. 26, no. 3, pp. 1835-1584, Jul. 2015